Revue des Composites et des Matériaux Avancés-Journal of Composite and Advanced Materials
Vol. 36, No. 2, April, 2026, pp. 433-444
Journal homepage: http://iieta.org/journals/rcma

Bioactivity and Antibacterial Performance of Bioactive Glass–Nano-Hydroxyapatite Composites

Khulood Haleem Yousif[1], Enas Muhi Hadi[1], Nehia Naema Hussein[2], Raid A. Ismail[3*]

[1] Department of Materials Science, University of Technology, Baghdad 10066, Iraq
[2] Department of Biotechnology, University of Technology, Baghdad 10066, Iraq
[3] Department of Laser Science and Technology, University of Technology, Baghdad 10066, Iraq

Corresponding Author Email: raidismail@yahoo.com

https://doi.org/10.18280/rcma.360219

Received: 18 February 2026
Revised: 10 April 2026
Accepted: 22 April 2026
Available online: 30 April 2026

Keywords:
bioactive glass, nano-hydroxyapatite, biocomposites, antibacterial activity, biofilm formation inhibition

ABSTRACT

Bioactive glass (BG) has attracted considerable attention as a promising material for biomedical applications. This study focuses on the development of BG–nHA biocomposites with enhanced biofunctional properties during the in-vitro assessment compared with previously reported systems. The sol–gel method is used to synthesize BG nanoparticles, and BG–nHA biocomposites were fabricated by dry pressing under hydraulic pressure using defined ratios of BG and nano-hydroxyapatite (nHA), followed by sintering at 1000 °C. The specimens were characterized before and after immersion in simulated body fluid (SBF) using Fourier Transform-Infrared Spectroscopy (FT-IR), Field Emission-Scanning Electron Microscopy (FE-SEM), X-ray diffraction (XRD), and weight loss measurements. Physical and mechanical properties, including apparent porosity, water absorption, apparent density, and hardness, were evaluated. At 25 wt.% nHA, the composite exhibited 31% porosity, 19% water absorption, 1.99 g/cm³ density, and a hardness of 388 HV. Results confirmed that a hydroxyapatite layer formed after SBF immersion, with increased apatite formation at higher nHA content. Increasing nHA content 5–25 wt.% enhanced both bioactivity and hardness of the BG–nHA composites. Moreover, antibiofilm tests confirmed that the BG–nHA biocomposites exhibited strong antibiofilm activity, with inhibition rates of 92.7% and 86.9% against Staphylococcus aureus and Klebsiella pneumoniae, respectively, indicating their suitability as promising bone-regeneration materials.

1. INTRODUCTION

The skeletal system is the most essential support structure that the human body possesses. It provides organ protection, blood cell formation, mineral storage, and body shape. Tissues are an essential part of the skeletal framework that support stability and safety during movement or rest [1]. The failure of bones, teeth, and joints results from the gradual deterioration of the skeletal system over time [2]. Bone defects may occur due to degenerative diseases, fractures, bone resection, or congenital defects. Small defects can be repaired through bone remodeling and healing within a relatively short time, whereas large (massive) defects are severe and difficult to recover, requiring bone reconstruction and surgical intervention [3, 4]. Recently, biomaterials have gained significant attention in implant production. Biomaterials are natural or synthetic substances used to replace or modify biological tissue functions. The usage of artificial materials to substitute damaged tissue and organs has become an essential field in modern medicine. Biomaterials are mainly classified into metals, ceramics, polymers, glasses, and composites [5, 6]. Bioceramic materials are important in biomedical applications such as dental materials, spinal cord repair, and orthopedic uses [7, 8], and play a key role in skeletal system reconstruction [9, 10]. Bioactive glass (BG) 45S5 is an amorphous bioceramic extensively utilized for bone regeneration, repair, and replacement due to its excellent osteogenic properties and biocompatibility [11, 12]. It consists mainly of silicon, calcium, sodium, and phosphate oxides, which enable strong bonding with bone tissue [13]. When BG interacts with biological environments, it promotes tissue adhesion and gradually degrades while new tissue forms, producing a biologically active apatite layer essential for bone bonding. This surface layer formation is a key factor in direct bone bonding [14, 15].

Hydroxyapatite (nHA) is an important inorganic bioceramic widely used in implant dentistry and bone implants according to its similarity with the minerals present in natural bone and tooth [16]. It is the primary inorganic component of bone, exhibiting distinct biologic compatibility, bioactivity, osteoconductive properties, bone bonding ability, and slow in situ degradation [17, 18]. The development of BG/nHA biocomposites is based on combining BG particles with nHA to improve biological activity, mechanical properties, and structural similarity to natural bone [19]. Antibacterial activity refers to the ability of a material to reduce bacterial survival, measured by colony-forming units before and after exposure [20]. Biofilms are surface-attached microbial communities formed by bacteria such as *Klebsiella pneumoniae*, *Staphylococcus aureus*, and *Pseudomonas aeruginosa*. Preventing biofilm formation is important, and nHA is considered a promising material for treating biofilm-associated infections because it is chemically similar to bone mineral [21].

In this study, BG/nHA biocomposites were prepared using the dry pressing method and characterized. The incorporation of nano-hydroxyapatite (nHA) into the BG 45S5 matrix improves mechanical stability, enhances hydroxyapatite layer formation, reduces brittleness, and increases surface area for better interaction with biological tissues. The physical, mechanical, and structural properties were evaluated. In vitro FTIR analysis confirmed the formation of an apatite layer that seemed like bone in simulated body fluid (SBF). Additionally, antibacterial and antibiofilm activities of BG/nHA biocomposites were investigated.

2. MATERIALS AND PROCEDURES

2.1 Fabrication of biocomposites

Bioactive glass powder (BG 45S5) with a composition of (45 wt.% SiO_2, 24.5 wt.% Na_2O, 24.5 wt.% CaO, and 6 wt.% P_2O_5) was synthesized using sol–gel method. Tetraethyl orthosilicate (23.5 mL) and Triethyl phosphate (3.35 mL) were added dropwise to an acidic solution (10.4 mL) under magnetic stirring. Sodium nitrate (16.5 g) and calcium nitrate tetrahydrate (15.5 g) were then added. The mixture was stirred for 1h until a clear solution was obtained. It was subsequently converted into gel via Polycondensation. The gel was dehydrated at 60 ℃ for 12h. After that, it was heat-treated for 5h at 200 ℃ and 2h at 700 ℃ to produce BG 45S5 powder.

Then, BG is mixed in several proportions (5, 10, 15, 20, and 25 wt.%) of nHA powder with particle size ±20 nm (Hualanchem, purity 96%, made in China). In order to ensure homogeneity and produce an appropriate ceramic, the mixture was stirred for 12h. The BG–nHA biocomposite specimens were produced using uniaxial pressing methods in hardened steel molds that were lubricated with paraffin oil under a compaction pressure of 312 MPa for 5 min to ensure a homogeneous compact. The resulting specimens were disc-shaped, with dimensions of 20 mm in diameter and 4 mm in thickness. No organic binder was added. The specimens were then sintered in a furnace (BSM-F40, China) at 1000 ℃ for 3 h with a heating rate of 5 ℃/min. In order to avoid thermal shock, furnace cooling occurred overnight at room temperature. This procedure is consistent with a previous study [22].

Table 1 illustrates the mixture ratios of BG and nHA used to prepare the biocomposite samples. The schematic diagram of the experimental set-up used to prepare biocomposite samples is shown in Figure 1.

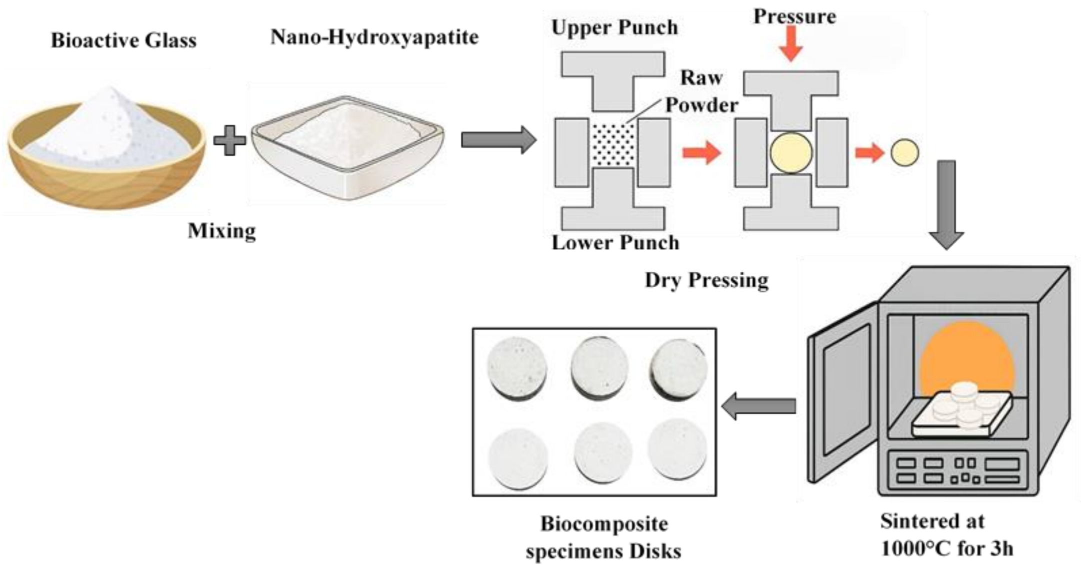

Figure 1. Schematic diagram of experimental set-up for preparation of biocomposite samples

Table 1. Mixture ratios of bioactive glass (BG) and nano-hydroxyapatite (nHA) used to prepare the biocomposite samples

Biocomposite Specimens Code	Composition of Each Element (wt.%)	
	Bioactive Glass (BG 45S5)	nHA
BG	100	0
BG–nHA1	95	5
BG–nHA2	90	10
BG–nHA3	85	15
BG–nHA4	80	20
BG–nHA5	75	25

Table 2. Simulated body fluid (SBF) ion concentrations in comparison to human blood plasma

Ions	SBF (mmol/l)	Human Blood Plasma (mmol/l)
Na^+	142.0	142.0
K^+	5.0	5.0
Mg^+	1.5	1.5
Ca^+	2.5	2.5
Cl^-	148.8	103.0
HCO_3^-	4.2	27.0
HPO_4^{2-}	1.0	1.0
SO_4^{2-}	0.5	0.5

2.2 Preparation of simulated bodily fluid

A simulated bodily fluid utilized in this investigation was procured commercially and prepared according to the methodology established by Kokubo and Takadama [23]. The solution's ion concentrations are illustrated in Table 2.

2.3 Surface morphology and particle size of BG powder and characterization of biocomposites BG–nHA

The particle size was determined for bioactive glass powder (BG 45S5) using a laser light diffraction instrument (Nano brook 90Plus, DLS). X-ray diffraction (XRD) analysis of the biocomposite specimens (BG–nHA) was performed using a diffractometer (PW1730, Philips, Netherlands) with Cu-Kα radiation (λ = 1.5405 Å). The diffraction patterns were recorded in the 2θ range of 20°–80° with a step size of 0.05°.

Fourier transform infrared (FT-IR) analysis of biocomposite specimens was carried out using an FT-IR spectrophotometer (PerkinElmer Spectrum IR-10.6.2, USA) coupled with an FT-IR imaging system in the range of 500–4000 cm^{-1}.

The surface morphology and topography of biocomposites were examined before and after immersion in SBF solution by using Field Emission-Scanning Electron Microscopy (FE-SEM) (MIRA 3 TESCAN, Czech).

Physical and mechanical properties of BG and BG–nHA biocomposite samples, namely**,** Apparent Porosity (A.P), Water Absorption ratio (W.A), and Apparent Density (A.D), were investigated according to ASTM C373-88 [24] and calculated by using these equations, respectively.

$$A.P = w_s - w_d/w_s - w_i \times 100\% \quad (1)$$

$$W.A = w_s - w_d/w_d \times 100\% \quad (2)$$

$$A.D = w_d/w_s - w_i \times \rho_w \quad (3)$$

where,

w_d: is the mass of the dried sample in grams.

w_s: sample mass under water infiltration (g).

w_i: sample mass submerged in water (g).

ρ_w: density of water ($g.cm^{-3}$).

Additionally, Vickers micro-hardness was assessed by applying a constant stress of 9.8 N for a duration of 10 seconds according to the American specifications ASTM C 1327-99. As in Eq. (4). All measurements were performed in triplicate, and the results are presented as mean ± SD.

$$HV = 1.854 \times F/a^2 \quad (4)$$

where,

HV: micro-hardness Vickers.

F: stands for the indentation load (N).

a: half of the diagonal indentation (mm).

1.854 is the value that represents the diamond pyramid's geometrical constant.

2.4 Biological evaluations

The pH change and weight loss of the biocomposite specimens were evaluated by immersing them in 100 ml of SBF solution and maintaining them in an incubation shaker at 37 °C for 1, 7, 14, 21, and 28 days. After each time point, the specimens were washed with distilled water to prevent any further reactions, and subsequently dried in an oven at 60 °C for up to 4 h. This procedure was used to determine biodegradation behavior and bioactivity in vitro. The pH of the SBF solution was measured at each time point using a digital pH meter (PH-600, Metravi, India). The weight of the biocomposite specimens was recorded before and after immersion in SBF.

The Antibacterial activity was determined using isolated bacteria of Gram-negative, such as (*P. aeruginosa and K. pneumoniae*), as well as Gram-positive (*S. aureus and S. mutans*), which were collected from the lab for microbiology at Medical City Hospital, Baghdad, Iraq. The isolates were characterised utilising the VITEK technology (VITEK, Biomérieux, Marcy-l'Etoile, France).

An antibacterial activity of purified BG, hydroxyapatite (nHA), and their combined mixture (BG/nHA) was evaluated using the agar well diffusion technique against selected pathogens. Bacterial suspensions were prepared at 1.5×10^8 CFU/mL using a McFarland standard, and Mueller-Hinton agar plates were inoculated with the test organisms. Wells of 6 mm diameter were created in the agar; each well was filled with BG and nHA powder suspensions with a concentration of 80 mg/mL, prepared from stock suspensions. The suspensions were separately dispersed by sonication for 2 min prior to use. The BG and nHA suspensions were then mixed in a 1:1 volume ratio. As a negative control, deionized water was utilized [25]. After incubating at 37 °C for 24 h, antibacterial activity of both pure BG and nHA, as well as their mixtures (biocomposites), was determined by examining and measuring the zones of inhibition in each well to the smallest millimeter. The increase in inhibition (F.I.) zones was calculated using Eq. (5):

$$F.I. = [(b - a)/a] \times 100\% \quad (5)$$

After that, antibiofilm activity was evaluated using the microtiter plate (MTP) technique to measure the inhibitory effect of BG–nHA biocomposites against biofilm formation [26]. A 96-well polystyrene MTP with a flat-bottom and sterile surface was employed. Biofilm development was initiated by bacterial adhesion to the well surface, and this process was influenced by the tested materials. Cultures of bacterial isolates were incubated on nutrient agar and activated at 37 °C overnight. The bacterial colonies were subsequently suspended in sterile normal saline solution and adjusted with a 0.5 McFarland standard (1.5×10^8 CFU/mL). Subsequently, 90 µL of Brain Heart Infusion (BHI) broth containing 2% of glucose was added to each well, and 10 µL of bacterial suspension was added. Following incubation, the plates were dried and the contents were removed. Non-adherent cells were then removed by washing the plates three times with sterile phosphate-buffered saline solution (PBS). After this, 150 µL of 1% crystal violet solution was added to each well and incubated at room temperature for 20 min. The wells were washed three times with PBS to eliminate the excess stain. The adherent cells were subsequently fixed and solubilized with 150 µL of 95% ethanol. All experiments were conducted in triplicate. The microplate reader was employed to measure the optical density (OD) of each well at 580 nm.

For growth curve analysis, 0.1 mg/ML of BG–nHA suspensions and 0.1 mL of bacterial suspension were mixed with 10 mL of nutrient broth in sterile tubes. The suspension of bacteria was produced from a culture that was left to grow for 24 hours and was diluted to a 0.5 McFarland standard.

Subsequently, 0.1 mL of the mixture was spread on Mueller-Hinton agar plates and incubated for 24 h at 37 °C. Viable bacterial growth was monitored at zero, 30, 60, 90, and 120 minutes to evaluate bacterial growth dynamics [27].

2.5. Statistical analysis

The data were analyzed using a one-way ANOVA procedure in SPSS Version 24, with a significance level of 0.05. Results are presented as mean ± standard error. All experiments were performed in triplicate.

3. RESULTS AND DISCUSSION

Figure 2 illustrates the morphology of the surface and distribution of particle sizes for BG 45S5 powder synthesized using the sol-gel method. Through the size distribution curve illustrated in Figure 2(a), the maximum intensity peak was obtained at 244 nm. Smaller particle sizes lead to higher surface reactivity and contribute to the rapid formation of the HA layer. Figure 2(b) shows the morphology of BG 45S5 synthesized by the sol-gel method using FE-SEM. The FE-SEM micrograph shows agglomeration of BG nanoparticles, which is attributed to their enhanced surface reactivity.

Figure 3 displays the XRD pattern of the BG–nHA biocomposite samples prepared at different nHA percentages. The XRD results show the main phases: Wollastonite ($CaSiO_3$) and hydroxyapatite, indicating partial crystallization of the synthesized BG at 1000 °C. Wollastonite was identified as a bioactive phase according to JCPDS #84-0655. Two distinct peaks of hydroxyapatite and wollastonite were selected for comparison. The HA peak was observed at 2θ = 40.54°, while Wollastonite was observed at 2θ = 34.14°. Formation of sodium calcium silicate $Na_2Ca(SiO_3)_2$ appears in the sintered samples at 1000 °C, consistent with JCPDS #77-2189. The results also suggest a possible transformation of HA into β-TCP after sintering, in agreement with reported studies [28]. The intensity of HA peaks increases as the nHA percentage increases, and this indicates that the HA crystallinity is higher. BG–nHA5 sample shows the highest Wollastonite content, suggesting a phase composition that may support hydroxyapatite formation on the BG surface during interaction with SBF.

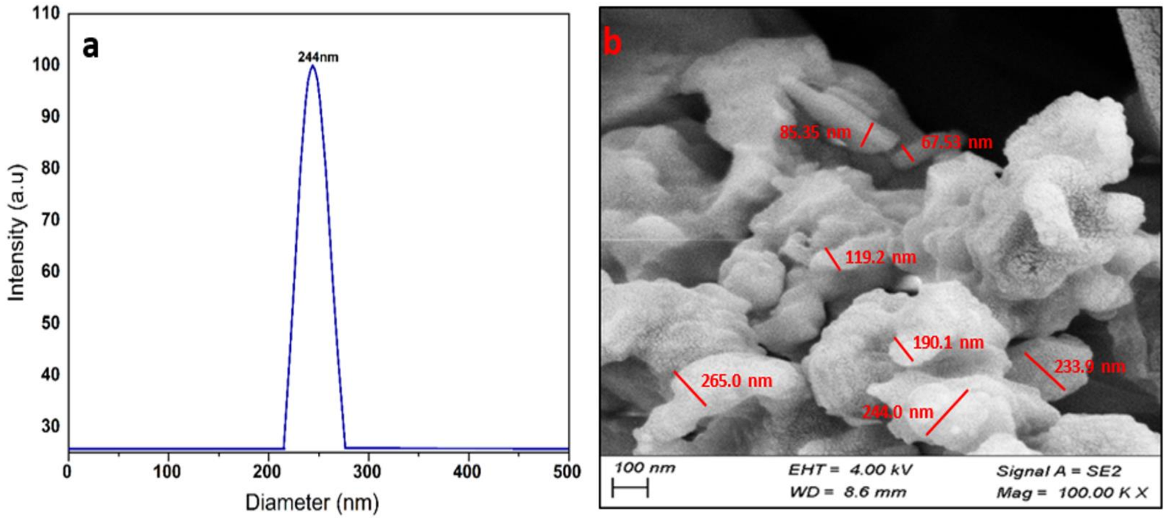

Figure 2. (a) Particle size analysis, (b) Field Emission-Scanning Electron Microscopy (FE-SEM) of 45S5 bioactive glass powder

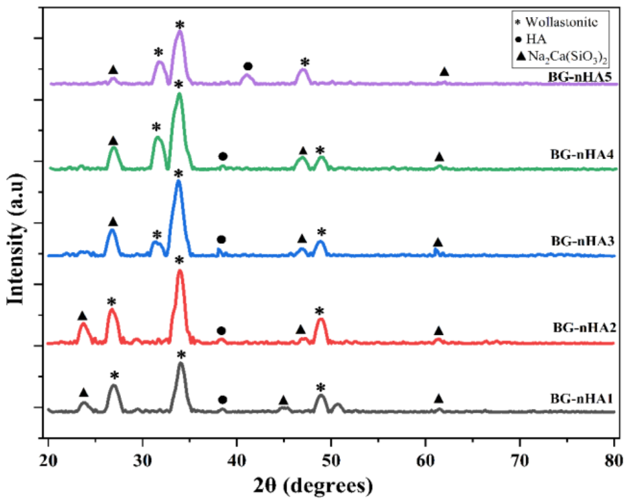

Figure 3. XRD of the BG–nHA biocomposite samples prepared at different nHA percentages

Note: XRD = X-ray diffraction, BG = bioactive glass, nHA = nano-hydroxyapatite

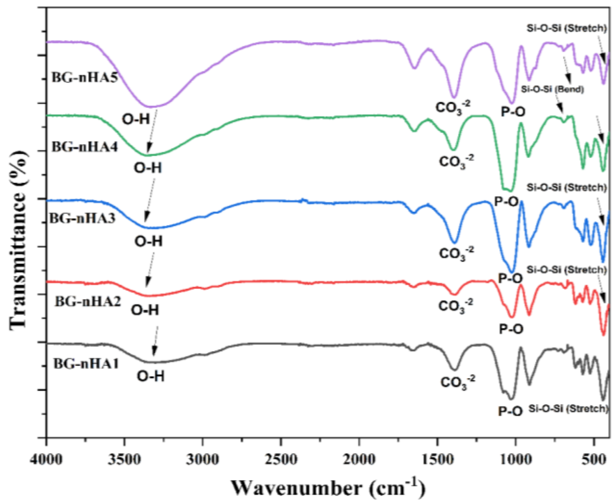

Figure 4. FT-IR spectrum of BG–nHA biocomposite specimens prepared before immersion in SBF

Note: FT-IR = Fourier Transform-Infrared Spectroscopy, BG = bioactive glass, nHA = nano-hydroxyapatite, SBF = simulated body fluid

Figure 4 shows the FT-IR spectrum of BG–nHA biocomposite specimens before soaking in SBF. FT-IR spectrum reveals the distinctive vibration bands of Si–O–Si, PO_4^{3-}, OH, and CO_3^{2-} groups. The band at 443 cm^{-1} is attributed to the symmetric stretching of Si–O–Si, while a band with 692 cm^{-1} is assigned for the bending vibration of Si–O–Si. The phosphate (PO_4^{3-}) band observed at 524, 620, 618, and 1035 cm^{-1} increases in intensity with increasing nHA content, indicating an increase in phosphate-related bonding within the composites. The broad bands at 3305–3552 cm^{-1} are attributed to hydroxyl (OH) groups. The Si–O–Si band is more pronounced in samples with higher bioactive glass (BG 45S5) content. As the HA content increases, the intensity of Si–O–Si decreases, while phosphate bands become more dominant due to the higher phosphate content in HA [29]. In addition, carbonate (CO_3^{2-}) bands at 1387–1394 cm^{-1} are observed, and their intensity increases with increasing HA content, consistent with previous studies [30].

Figure 5 shows the FT-IR Spectrum of (BG–nHA) Biocomposite specimens after immersion in SBF. Compared to the spectra obtained before the soaking, there is a clear difference.

After immersion, the bands of phosphate (P–O) at 576, 918, and 1039 cm^{-1} become more pronounced, indicating an increase in the apatite phase because a calcium phosphate layer formed on the specimen surface. In contrast, Si–O bands at 532, 690, and 732 cm^{-1} decrease in intensity, suggesting that the bioactive glass surface is gradually covered by the newly formed apatite layer. The carbonate bands at 1427–1456 cm^{-1} become more evident after soaking, indicating the formation of carbonated apatite, similar to natural bone mineral. The hydroxyl band in the range of 3400–3450 cm^{-1} shows increased intensity with a slight shift to higher wavenumbers, which is associated with additional hydroxyl groups formed during apatite precipitation on the surface. The increase in phosphate and carbonate bands after SBF soaking confirms the formation of an apatite layer that likely forms bone and enhances the bioactivity of BG–nHA biocomposites, supporting their suitability for bone tissue engineering applications, consistent with previous studies [30, 31]. FT-IR assignments of BG–nHA samples before and after soaking in SBF are summarized in Table 3.

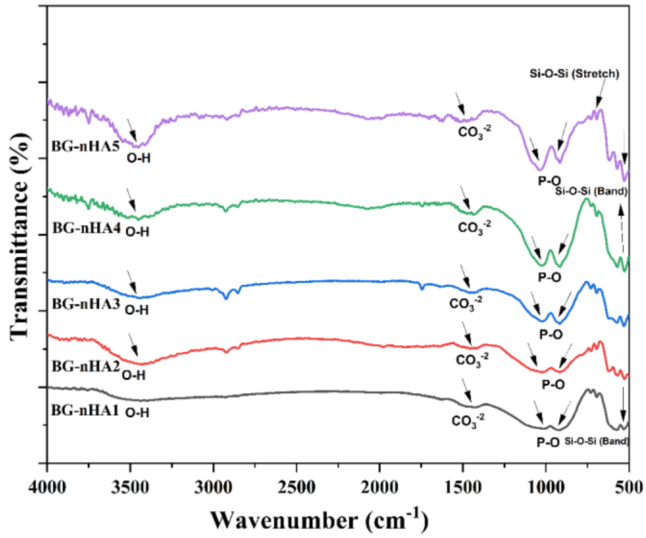

Figure 5. FT-IR spectrum of BG–nHA biocomposite specimens prepared after immersion in SBF

Note: FT-IR = Fourier Transform-Infrared Spectroscopy, BG = bioactive glass, nHA = nano-hydroxyapatite, SBF = simulated body fluid

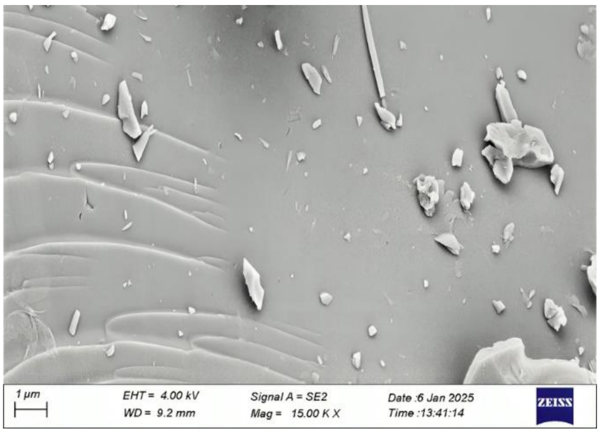

(a) BG

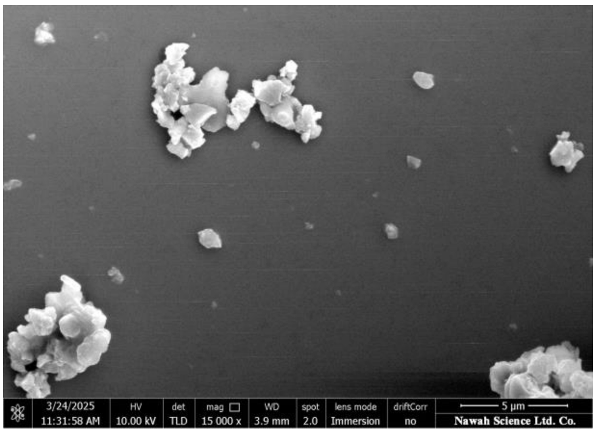

(b) BG–nHA1

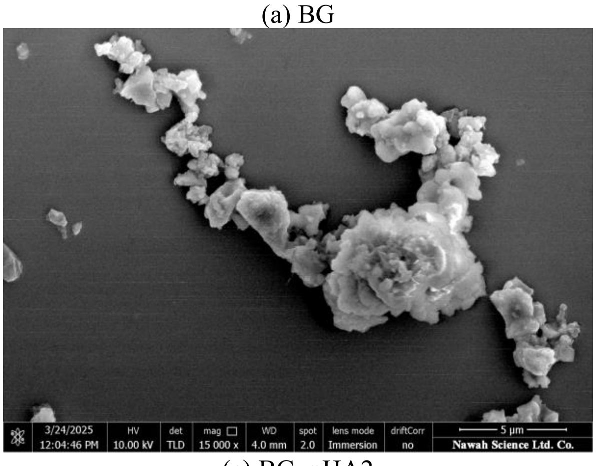

(c) BG–nHA2

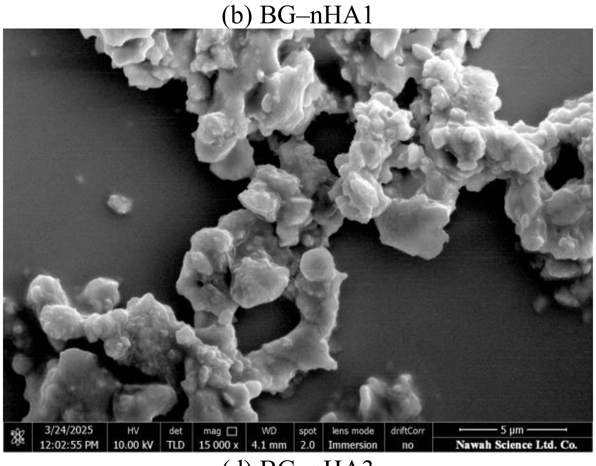

(d) BG–nHA3

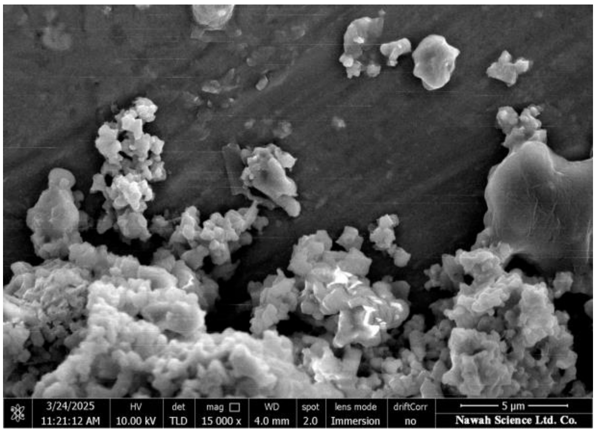

(e) BG–nHA4

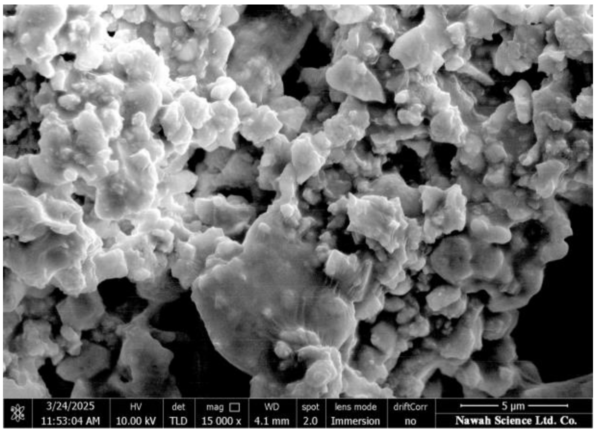

(f) BG–nHA5

Figure 6. FE-SEM images of bioactive glass and the biocomposite disks BG–nHA specimens before immersion in SBF
Note: FE-SEM = Field Emission-Scanning Electron Microscopy, BG = bioactive glass, nHA = nano-hydroxyapatite, SBF = simulated body fluid

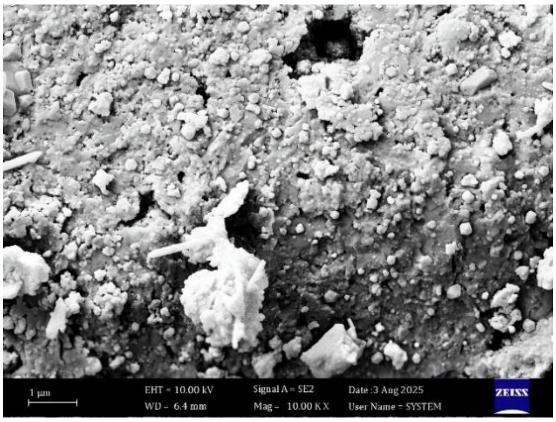

(a) BG

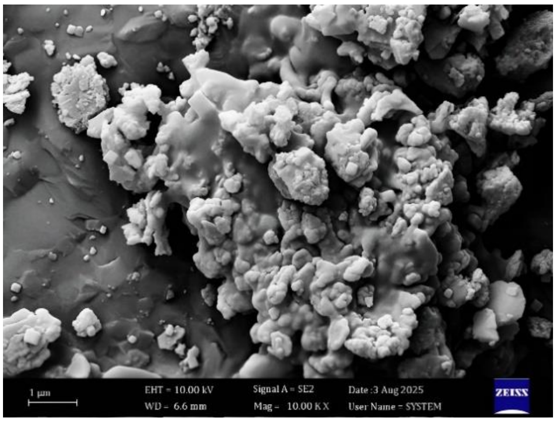

(b) BG–nHA1

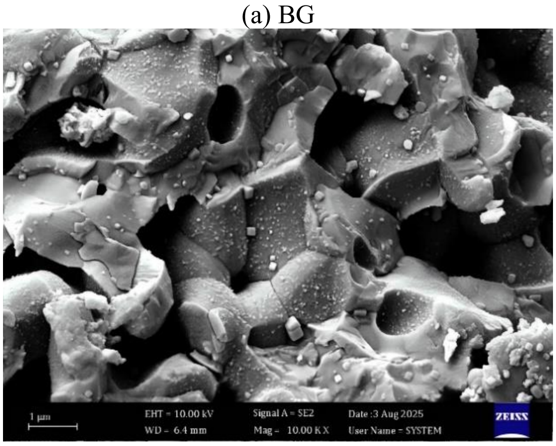

(c) BG–nHA2

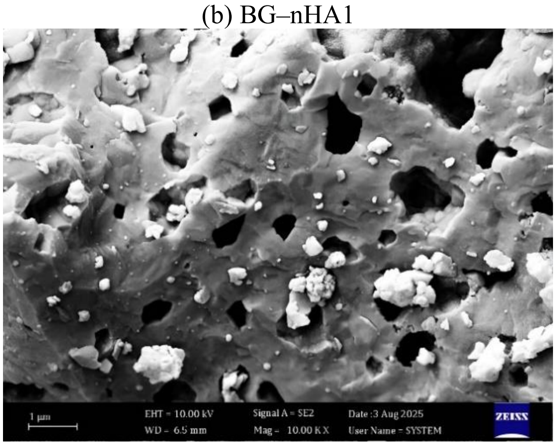

(d) BG–nHA3

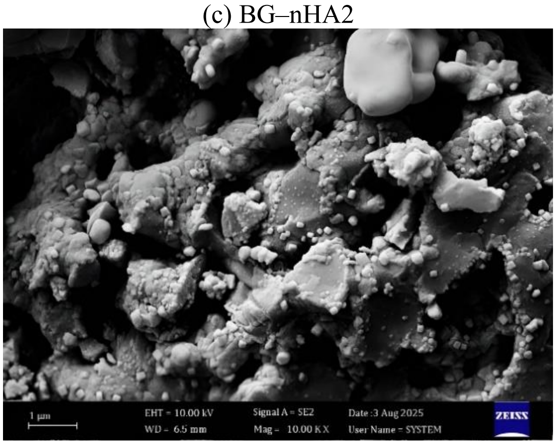

(e) BG–nHA4

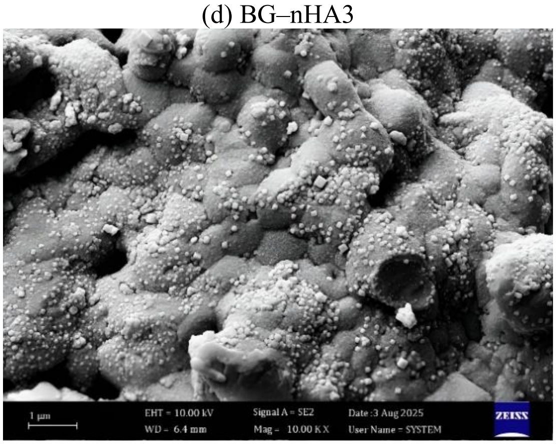

(f) BG–nHA5

Figure 7. FE-SEM images of bioactive glass and biocomposite disks BG–nHA specimens after 28 days of immersion in SBF
Note: FE-SEM = Fourier Transform-Infrared Spectroscopy, BG = bioactive glass, nHA = nano-hydroxyapatite, SBF = simulated body fluid

Table 3. FT-IR assignments of biocomposite BG–nHA specimens before and after soaking in SBF

Bands	Wavenumber cm^{-1} Before Soaking	Wavenumber cm^{-1} After Soaking
Si–O–Si symmetric stretching	443	690, 732
Si–O–Si vibration bending	692	532
P–O	524, 620, 618, 1035	576, 918, 1039
Carbonate groups (CO_3^{2-})	1387-1394	1427-1456
Hydroxyl group	3305-3352	3400-3450

Note: FT-IR = Fourier Transform-Infrared Spectroscopy, BG = bioactive glass, nHA = nano-hydroxyapatite, SBF = simulated body fluid

Figures 6 and 7 demonstrate the surface morphology of a BG and the prepared biocomposite specimens (BG–nHA) prior to and after soaking in SBF, respectively.

In Figure 6, FE-SEM images show the presence of specific quantities of porosity, glassy phase, and HA matrix layers. Additionally, it is observed that heterogeneous surfaces are composed of particulates with sharp edges and different sizes. Furthermore, the nHA ratio increases, indicating an increase in the distribution of P, which is a representative of nHA in the biocomposites, and Si, which is associated with the BG, which decreases.

SEM images of the samples immersed in SBF exhibit the formation of irregular shapes and the growth of grounded nHA particles. The images demonstrate that a high concentration of BG in the specimens' contents contributed to the development of apatite particles on the external surface [32]. BG–nHA specimens that were immersed in SBF for 28 days exhibited clear spherical apatite crystals on their external surfaces (Figure 7).

The biocomposites (Figure 7(b)-(d)) exhibit a melted and dense structure due to the high content of silica, which decreases the nucleation process of an apatite layer compared to other composites. FE-SEM images show that the composite has a significant amount of particles on its surface, which demonstrates that the apatite layer has formed slightly. Additionally, as clearly shown in Figure 7(e), the FE-SEM image shows the existence of rich spherical shapes stacked over one another to produce an apatite layer that is similar to bone.

The apparent porosity and apparent density as an indicator of nHA contents are presented in Figure 8(a), which demonstrates that an increase in the amount of hydroxyapatite results in a decrease in the porosity, and the concentration of the pores in biocomposite specimens decreased compared to those without the nHA. The finding can be explained on the basis that the hydroxyapatite particles increased the compactness and enhanced the particles' bonding. Furthermore, decreasing the biocomposites' apparent porosity may be related to the higher density of HA in comparison to that of BG and its ability to fill the voids between the BG particles, which is consistent with reported data [33, 34].

The water absorption percentage decreased as the nHA content increased, due to the reduction in porosity percentage as shown in Figure 8(b). The Biocomposites with a higher BG ratio have a higher water absorption ratio compared to those without nHA. This is due to the fact that the BG sample contains Si–O–Si groups, which enhance hydration when immersed in water and increase its water absorption capacity.

As is obvious in Figure 9, the findings indicated that the Vickers micro-hardness increased with higher nHA contents before immersion, attributed to the lower apparent porosity. Hardness is directly related to density; as density increases, porosity decreases. This is consistent with the results of research [35, 36].

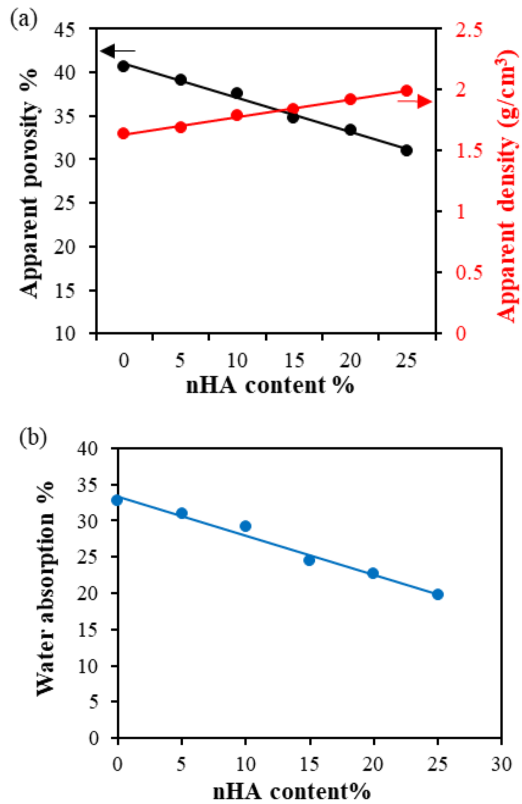

Figure 8. Effects of nHA ratio on (a) apparent porosity and apparent density, and (b) water absorption ratio of biocomposite samples

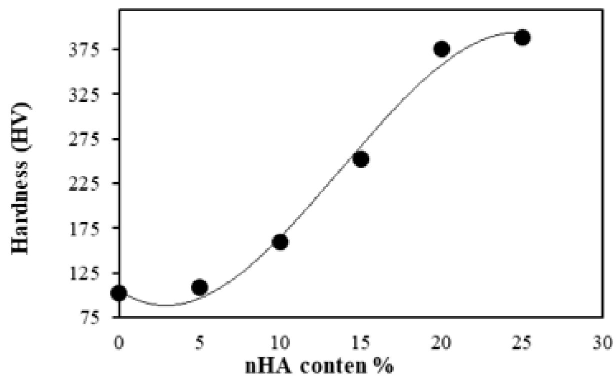

Figure 9. Micro-hardness versus nHA content plot of biocomposites BG–nHA samples before immersion in SBF

Figure 10 shows the effect of immersion time in SBF solution on pH value and weight loss after immersion of the biomolecules (BG–nHA). After one day of immersion, all samples exhibited a significant increase in pH value, which was subsequently followed by a slight decrease in pH value after an extended ageing period of up to 28 days.

The pH variation is mainly attributed to ion exchange reactions at the BG surface. Cations such as (Na^+ and Ca^{2+}) diffuse into a solution, while (H^+ or H_3O^+) ions from the surrounding medium are incorporated into the glass structure, leading to an increase in pH [37]. The subsequent decrease in pH is associated with the precipitation of calcium phosphate and carbonate compounds. This occurs as equilibrium shifts toward the formation of solid phases, consuming carbonate and phosphate ions from the solution, which results in pH reduction.

During immersion in SBF, surface reactions are influenced by the incorporation of nHA into the BG matrix. This enhances nucleation and growth of the hydroxyapatite layer over time, showing behavior consistent with previous studies [38].

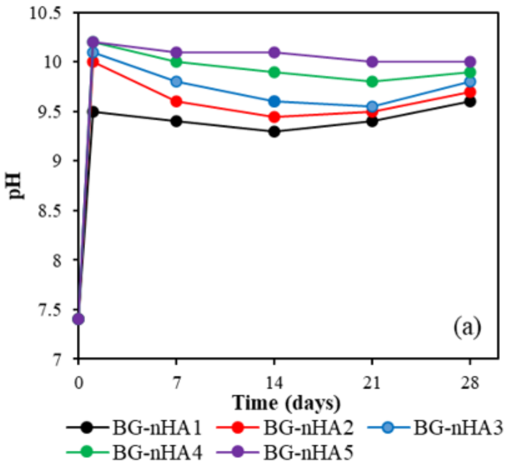

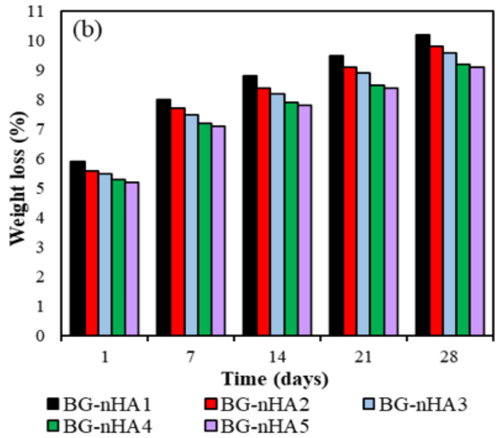

Figure 10. (a) pH variation with SBF immersion period and (b) weight loss histogram with SBF immersion duration of samples prepared with different nHA contents

Figure 10(b) shows the weight loss behavior of the biocomposites. A rapid weight loss is observed in the early immersion period, followed by a relatively stable trend up to 7 days. The surface becomes stabilized due to the formation of an apatite layer, which develops during soaking in SBF. This continues until minimal weight change is observed. The presence of calcium phosphate in the composites promotes hydroxyapatite formation in SBF and enhances the development of the hydroxyapatite layer after immersion, consistent with previous reports [39].

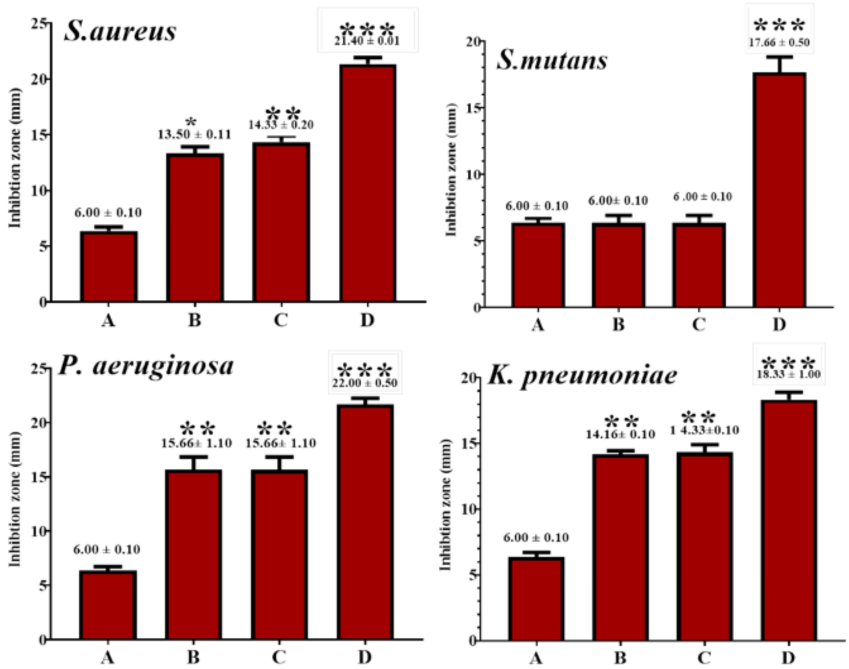

Figure 11. Antibacterial activity of biocomposites BG–nHA against four types of pathogenic bacteria: *S. aureus*, *S. mutans*, *P. aeruginosa*, and *K. pneumoniae*

Note: BG = bioactive glass, nHA = nano-hydroxyapatite

Table 4. Antibacterial activity of BG, nHA, and BG–nHA biocomposite samples against four types of pathogenic bacteria

Bacteria Isolates	A	B	C	D	F.I.% of BG–nHA1	F.I.% of BG–nHA2
S. aureus	6.00	21.33 ± 1.52	14.33 ± 1.52	13.33 ± 2.51	-60.01%	-7.5%
S. mutans	6.00	17.66 ± 3.05	6.00 ± 0.0	6 ± 0.0	-194.33%	0.0%
P. aeruginosa	6.00	22 ± 0.0	15.66 ± 3.08	15.66 ± 3.08	-40.48%	0.0%
K. pneumoniae	6.00	18.33 ± 1.52	14 ± 2	14.66 ± 2.08	-25.03%	4.5%

Note: A = Control, B = BG, C = nHA, D = BG–nHA; BG = bioactive glass, nHA = nano-hydroxyapatite, SBF = simulated body fluid, F.I. = formation inhibition

Figure 11 and Table 4 demonstrate the results of the antibacterial activity of BG–nHA specimens against four types of pathogenic bacteria. The results show that the highest effect was observed with BG alone in the growth of all pathogenic bacterial species, followed by nHA. When the two substances were mixed, the BG–nHA composites showed reduced inhibition compared to pure BG, indicating an antagonistic effect of the binary mixture. This behavior is mainly attributed to the reduced BG content in the biocomposite matrix, which decreases the release of ions (Ca^{2+} and silicate ions) and limits the increase in pH responsible for antibacterial activity [40]. In contrast, nHA is generally biologically inert in terms of antibacterial activity and shows limited direct contribution to bacterial inhibition. Its nanoparticulate form may enable electrostatic interactions with bacterial cell walls [41], but this effect remains weaker compared to the ion-release mechanism of BG. Therefore, nHA incorporation reduces the overall antibacterial performance due to dilution of BG activity. However, it improves other important properties such as mechanical strength and osteoconductivity, consistent with previous studies [42]. This was demonstrated by the negative percentage (F.I) %. The finding showed a highly statistically significant result at a value of ($p < 0.0001$). An antagonistic effect is observed when the combined effect of two agents is lower than their individual effects when used separately, a well-known phenomenon in pharmacology [43]. The reduced antibacterial performance of the BG–nHA system is consistent with this behavior.

Antibiofilm formation activity for BG–nHA samples showed a maximum anti-biofilm activity of 92.7% and 86.9% against *S. aureus* and *K. pneumonia*, respectively. Additionally, BG–nHA significantly reduced biofilm formation in all tested bacteria, as illustrated in (Figure 12(e) and (f)), indicating strong anti-biofilm performance.

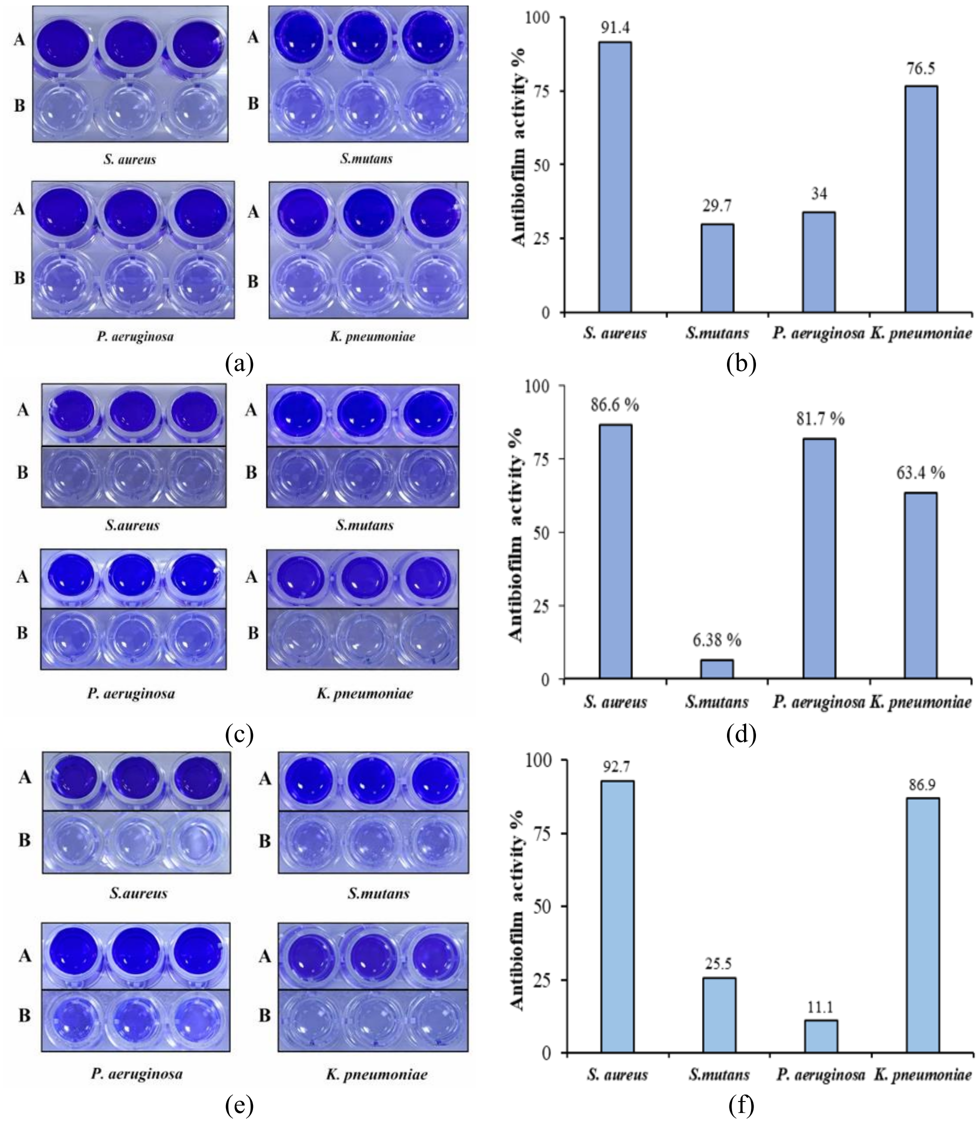

Figure 12. Antibiofilm activity of (a) BG, (b) BG inhibiting the ability of bacteria to form a biofilm, (c) nHA, (d) nHA inhibiting the ability of bacteria to form a biofilm, (e) BG–nHA, and (f) BG–nHA inhibiting the ability of bacteria to form a biofilm
Note: A- before treatment, B- after treatment; BG = bioactive glass, nHA = nano-hydroxyapatite

This effect is attributed to the partial dissolution of BG–nHA in aqueous environments, leading to the release of (Na^{+}, Ca^{2+}, Si^{4+}, and PO_4^{3-}) ions. This ionic release increases pH and osmotic pressure, creating an unfavorable environment for bacterial growth [44, 45].

Furthermore, the presence of nHA contributes to the anti-biofilm activity by interfering with bacterial cell wall formation and growth through electrostatic interactions, reactive oxygen species formation, and possible penetration into bacterial cells [46]. BG–nHA biocomposites effectively reduce bacterial adhesion and biofilm mass, demonstrating potential for preventing biofilm-associated infections in biomaterial applications.

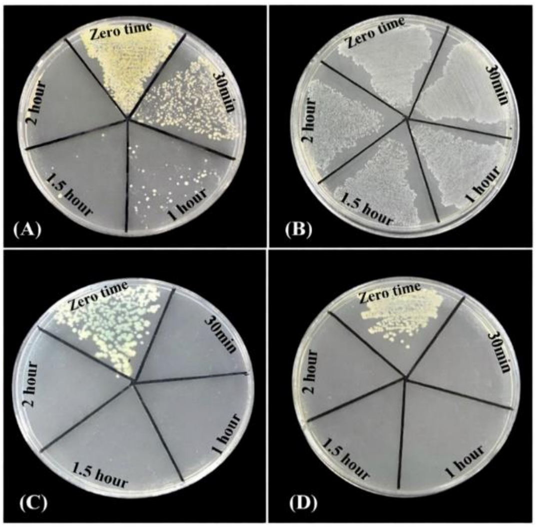

Figure 13. Growth curve assay of biocomposites BG–nHA samples against (A) *S.aureus*, (B) *S. mutans*, (C) *P. aeruginosa*, and (D) *K. pneumoniae*
Note: BG = bioactive glass, nHA = nano-hydroxyapatite

Figure 13 shows a decrease in bacterial colony numbers of *P. aeruginosa* and *K. pneumoniae* within the first 30 min of exposure to BG–nHA. For *S. aureus*, the colony counts were initially high but gradually decreased over time, reaching very low levels after 60 min, indicating a time-dependent antibacterial effect. In contrast, *S. mutans* exhibited clear resistance to this mixture. This resistance may be attributed to insufficient exposure duration and particle concentration, as well as to inherent defense mechanisms.

4. CONCLUSION

The dry pressing method and sintering process were utilized to produce an advanced BG–nHA biocomposite exhibiting enhanced mechanical properties and biological performance. An increasing amount of nano-hydroxyapatite 5, 10, 15, 20, and 25 wt.% was incorporated into the BG matrix to enhance bioactivity. The biocomposite containing 25 wt.% nHA and 75 wt.% BG showed the highest weight loss (9.1%), density (1.99 g/cm³), and hardness (388 HV). In addition, the biocomposite exhibited antibiofilm activity of 92.7% and 86.9% against *S. aureus* and *K. pneumoniae*, respectively. According to these in vitro findings, the BG–nHA biocomposites demonstrated enhanced biofunctional performance, indicating their potential as biomaterials for biomedical applications.

REFERENCES

[1] Clarke, B. (2008). Normal bone anatomy and physiology. Clinical Journal of the American Society of Nephrology, 3(S3): S131-S139. https://doi.org/10.2215/cjn.04151206

[2] Strnad, Z., Sestak, J. (1999). Bio-compatible ceramics as mimetic material for bone tissue substitution. In Proceedings of the Second International Conference on Intelligent Processing and Manufacturing of Materials. IPMM'99 (Cat. No.99EX296), Honolulu, HI, USA, pp. 431-436. https://doi.org/10.1109/ipmm.1999.792518

[3] Al-Qaysi, M. (2018). Development of phosphate based glass scaffolds for the repair of craniofacial bone. Doctoral dissertation, University College London.

[4] Kim, S.K., Murugan, S.S., Dalavi, P.A., Gupta, S., Anil, S., Seong, G.H., Venkatesan, J. (2022). Biomimetic chitosan with biocomposite nanomaterials for bone tissue repair and regeneration. Beilstein Journal of Nanotechnology, 13: 1051-1067. https://doi.org/10.3762/bjnano.13.92

[5] Rubežić, M.Z., Krstić, A.B., Stanković, H.Z., Ljupković, R.B., Ranđelović, M.S., Zarubica, A.R. (2020). Different types of biomaterials: Structure and application: A short review. Advanced Technologies, 9(1): 69-79.

[6] Saad, S.M., Hadi, E.M., Hussien, N.N. (2022). Zirconia–yttria system for manufacturing ceramic dental. International Journal of Nanoelectronics and Materials, 15: 37-47.

[7] Habraken, W.J.E.M., Wolke, J.G.C., Jansen, J.A. (2007). Ceramic composites as matrices and scaffolds for drug delivery in tissue engineering. Advanced Drug Delivery Reviews, 59(4-5): 234-248. https://doi.org/10.1016/j.addr.2007.03.011

[8] Saad, S.M., Hussien, N.N., Hadi, E.M. (2024). Enhancing the mechanical qualities of dental ceramics based on nano zirconia and yttria and other additive materials. AIP Conference Proceedings, 2922: 050001. https://doi.org/10.1063/5.0183665

[9] Vallet-Regí, M., Salinas, A.J. (2019). Ceramics as bone repair materials. In Bone Repair Biomaterials, pp. 141-178. https://doi.org/10.1016/b978-0-08-102451-5.00006-8

[10] Gao, Y., Seles, M.A., Rajan, M. (2023). Role of bioglass derivatives in tissue regeneration and repair: A review. Reviews on Advanced Materials Science, 62(1): 20220318. https://doi.org/10.1515/rams-2022-0318

[11] Gerhardt, L.C., Boccaccini, A.R. (2010). Bioactive glass and glass-ceramic scaffolds for bone tissue engineering. Materials, 3(7): 3867-3910. https://doi.org/10.3390/ma3073867

[12] Chen, Q.Z., Li, Y., Jin, L.Y., Quinn, J.M.W., Komesaroff, P.A. (2010). A new sol-gel process for producing Na2O-containing bioactive glass ceramics. Acta Biomaterialia, 6(10): 4143-4153. https://doi.org/10.1016/j.actbio.2010.04.022

[13] Izquierdo-Barba, I., Conde, F., Olmo, N., Lizarbe, M.A., García, M.A., Vallet-Regí, M. (2006). Vitreous SiO2-CaO coatings on Ti6Al4V alloys: Reactivity in simulated body fluid versus osteoblast cell culture. Acta Biomaterialia, 2(4): 445-455. https://doi.org/10.1016/j.actbio.2006.02.002

[14] Olmo, N., Martín, A.I., Salinas, A.J., Turnay, J., Vallet-Regí, M., Lizarbe, M.A. (2003). Bioactive sol-gel glasses with and without a hydroxycarbonate apatite layer as substrates for osteoblast cell adhesion and proliferation. Biomaterials, 24(20): 3383-3393. https://doi.org/10.1016/S0142-9612(03)00200-X

[15] Stanciu, G.A., Sandulescu, I., Savu, B., Stanciu, S.G., et al. (2007). Investigation of the hydroxyapatite growth on bioactive glass surface. Journal of Biomedical & Pharmaceutical Engineering, 1(1): 34-39.

[16] Ismail, R.A., Hamoudi, W.K., Abbas, H.F. (2018). Electrophoretic deposition of hydroxyapatite-shrimp

crusts nanocomposite thin films for bone implant studies. IET Nanobiotechnology, 12(6): 714-721. https://doi.org/10.1049/iet-nbt.2017.0272

[17] Abdulhussein, H.J., Mohsin, M.H., Jabir, M.S., Sulaiman, G.M., Mohammed, H.A., Ismail, R.A., Ramizy, A., Eisa, M.H., Ibrahim, N.A., Badher, N.S. (2025). Eco-friendly synthesis of eggshell-derived nano-hydroxyapatite: Physicochemical characterization, hemocompatibility, and bone regeneration potential. Scientific Reports, 15(1): 32832. https://doi.org/10.1038/s41598-025-17486-0

[18] Ismail, R.A., Salim, E.T., Hamoudi, W.K. (2013). Characterization of nanostructured hydroxyapatite prepared by Nd: YAG laser deposition. Materials Science and Engineering: C, 33(1): 47-52. https://doi.org/10.1016/j.msec.2012.08.002

[19] Zarifah, N.A., Matori, K.A., Sidek, H.A.A., Wahab, Z.A., Salleh, M.A.M., Zainuddin, N., Khiri, M.Z.A., Farhana, N.S., Omar, N.A.S. (2016). Effect of hydroxyapatite reinforced with 45S5 glass on physical, structural and mechanical properties. Procedia Chemistry, 19: 30-37. https://doi.org/10.1016/j.proche.2016.03.008

[20] Cai, J., Liu, R. (2020). Introduction to antibacterial biomaterials. Biomaterials Science, 8(24): 6812-6813. https://doi.org/10.1039/d0bm90100h

[21] Arunachalam, K., Davoodbasha, M. (2021). Imaging bacteria and biofilm by field emission scanning electron microscopy. In Analytical Methodologies for Biofilm Research, pp. 205-222. https://doi.org/10.1007/978-1-0716-1378-8_9

[22] Vafa, E., Bazargan-Lari, R., Bahrololoom, M.E. (2021). Synthesis of 45S5 bioactive glass-ceramic using the sol-gel method, catalyzed by low concentration acetic acid extracted from homemade vinegar. Journal of Materials Research and Technology, 10: 1427-1436. https://doi.org/10.1016/j.jmrt.2020.12.093

[23] Kokubo, T., Takadama, H. (2006). How useful is SBF in predicting in vivo bone bioactivity? Biomaterials, 27(15): 2907-2915. https://doi.org/10.1016/j.biomaterials.2006.01.017

[24] ASTM C373-88. (2006). Standard test method for water absorption, bulk density, apparent porosity, and apparent specific gravity of fired whiteware products. ASTM International, United States. https://store.astm.org/c0373-88r06.html.

[25] Muhammad, F., Hussein, N.N., Sulaiman, G.M. (2023). Potentials of iron oxide nanoparticles (Fe3O4): As antioxidant and alternative therapeutic agent against common multidrug-resistant microbial species. Iraqi Journal of Science, 64(6): 2759-2773. https://doi.org/10.24996/ijs.2023.64.6.10

[26] Abdul-Jabbar, A.M., Hussian, N.N., Mohammed, H.A., Aljarbou, A., Akhtar, N., Khan, R.A. (2022). Combined anti-bacterial actions of lincomycin and freshly prepared silver nanoparticles: Overcoming the resistance to antibiotics and enhancement of the bioactivity. Antibiotics, 11(12): 1791. https://doi.org/10.3390/antibiotics11121791

[27] Hamid, M.T., Hussein, N.N., Sulaiman, G.M., Mohammed, H.A. (2025). Antibacterial and antibiofilm properties of silver nanoparticles synthesized using Carthamus tinctorius extract against various multidrug-resistant bacterial strains. Discover Applied Sciences, 7(6): 548. https://doi.org/10.1007/s42452-025-06986-3

[28] Sebdani, M.M., Fathi, M.H. (2012). Preparation and characterization of hydroxyapatite-forsterite-bioactive glass nanocomposite coatings for biomedical applications. Ceramics International, 38(2): 1325-1330. https://doi.org/10.1016/j.ceramint.2011.09.008

[29] Ravarian, R., Moztarzadeh, F., Hashjin, M.S., Rabiee, S.M., Khoshakhlagh, P., Tahriri, M. (2010). Synthesis, characterization and bioactivity investigation of bioglass/hydroxyapatite composite. Ceramics International, 36(1): 291-297. https://doi.org/10.1016/j.ceramint.2009.09.016

[30] Prasad, S., Vyas, V.K., Ershad, M., Pyare, R. (2016). In vitro bioactivity and physical-mechanical properties of HA based 45S5 bio-composites. Key Engineering Materials, 702: 83-90. https://doi.org/10.4028/www.scientific.net/kem.702.83

[31] Ebrahimi, S., Sipaut, C.S. (2022). Synthesis of hydroxyapatite/bioglass composite nanopowder using design of experiments. Nanomaterials, 12(13): 2264. https://doi.org/10.3390/nano12132264

[32] Lin, K.S., Tseng, Y.H., Mou, Y., Hsu, Y.C., Yang, C.M., Chan, J.C.C. (2005). Mechanistic study of apatite formation on bioactive glass surface using 31P solid-state NMR spectroscopy. Chemistry of Materials, 17(17): 4493-4501. https://doi.org/10.1021/cm050654c

[33] Pinchuk, N., Parkhomey, O., Sych, O. (2017). In vitro investigation of bioactive glass-ceramic composites based on biogenic hydroxyapatite or synthetic calcium phosphates. Nanoscale Research Letters, 12(1): 111. https://doi.org/10.1186/s11671-017-1895-1

[34] Mirparizi, M. (2026). Coupled thermo-physical processes in porous phase-change energy storage systems with hybrid nanofluids. Journal of Complex and Multiphysics Engineering Systems, 1(1): 70-81. https://doi.org/10.56578/jcmes010104

[35] Shikimaka, O., Bivol, M., Sava, B.A., Dumitru, M., Tardei, C., Sbarcea, B.G., Grabco, D., Pyrtsac, C., Topal, D., Prisacaru, A., Cobzac, V., Nacu, V. (2022). Hydroxyapatite-bioglass nanocomposites: Structural, mechanical, and biological aspects. Beilstein Journal of Nanotechnology, 13: 1490-1504. https://doi.org/10.3762/bjnano.13.123

[36] Fragassa, C., Massimo, S., Arru, M., Pavlovic, A. (2026). Thermo-mechanical response of an automotive power module heat sink under combined thermal and power cycling. Journal of Complex and Multiphysics Engineering Systems, 1(2): 122-137. https://doi.org/10.56578/jcmes010201

[37] Hammami, I., Jakka, S.K., Sá-Nogueira, I., Borges, J.P., Graça, M.P.F. (2024). The effect of iron oxide insertion on the in vitro bioactivity, and antibacterial properties of the 45S5 bioactive glass. Biomimetics, 9(6): 325. https://doi.org/10.3390/biomimetics9060325

[38] Kaur, G., Pickrell, G., Kimsawatde, G., Homa, D., Allbee, H.A., Sriranganathan, N. (2014). Synthesis, cytotoxicity and hydroxyapatite formation in 27-Tris-SBF for sol-gel based CaO-P2O5-SiO2-B2O3-ZnO bioactive glasses. Scientific Reports, 4(1): 4392. https://doi.org/10.1038/srep04392

[39] Manafi, S., Mirjalili, F., Reshadi, R. (2019). Synthesis and evaluation of the bioactivity of fluorapatite-45S5 bioactive glass nanocomposite. Progress in Biomaterials, 8(2): 77-89. https://doi.org/10.1007/s40204-019-0112-y

[40] Ghomi, H., Fathi, M.H., Edris, H. (2012). Effect of the composition of hydroxyapatite/bioactive glass nanocomposite foams on their bioactivity and mechanical properties. Materials Research Bulletin, 47(11): 3523-3532. https://doi.org/10.1016/j.materresbull.2012.06.066
[41] Hassanain, M., Abdel-Ghafar, H.M., Hamouda, H.I., El-Hosiny, F.I., Ewais, E.M.M. (2024). Enhanced antimicrobial efficacy of hydroxyapatite-based composites for healthcare applications. Scientific Reports, 14(1): 26426. https://doi.org/10.1038/s41598-024-76088-4
[42] Seyedmajidi, S., Rajabnia, R., Seyedmajidi, M. (2018). Evaluation of antibacterial properties of hydroxyapatite/bioactive glass and fluorapatite/bioactive glass nanocomposite foams as a cellular scaffold of bone tissue. Journal of Laboratory Physicians, 10(3): 265-270. https://doi.org/10.4103/jlp.jlp_167_17
[43] Ocampo, P.S., Lázár, V., Papp, B., Arnoldini, M., Abel zur Wiesch, P., Busa-Fekete, R., Fekete, G., Pál, C., Ackermann, M., Bonhoeffer, S. (2014). Antagonism between bacteriostatic and bactericidal antibiotics is prevalent. Antimicrobial Agents and Chemotherapy, 58(8): 4573-4582. https://doi.org/10.1128/aac.02463-14
[44] Araujo, M.S., Silva, A.C., Cabal, B., Bartolomé, J.F., Mello-Castanho, S. (2021). In vitro bioactivity and antibacterial capacity of 45S5 Bioglass®-based compositions containing alumina and strontium. Journal of Materials Research and Technology, 13: 154-161. https://doi.org/10.1016/j.jmrt.2021.04.053
[45] Wanitwisutchai, T., Monmaturapoj, N., Srisatjaluk, R.L., Subannajui, K., Anuwongnukroh, N., Dechkunakorn, S., Pongprueksa, P. (2019). Antibacterial properties among different concentration of bioactive glasses. Key Engineering Materials, 814: 349-353. https://doi.org/10.4028/www.scientific.net/kem.814.349
[46] Neelakandeswari, N., Sangami, G., Dharmaraj, N. (2011). Preparation and characterization of nanostructured hydroxyapatite using a biomaterial. Synthesis and Reactivity in Inorganic, Metal-Organic, and Nano-Metal Chemistry, 41(5): 513-516. https://doi.org/10.1080/15533174.2011.568434